



*Journal of Applied Fluid Mechanics*, Vol. 10, No. 1, pp. 81-94, 2017.  
Available online at [www.jafmonline.net](http://www.jafmonline.net), ISSN 1735-3572, EISSN 1735-3645.  
DOI: 10.18869/acadpub.jafm.73.238.25947

## Numerical Investigation of Temporal Variation of Density Flow and Parameters

F. Üneş<sup>1†</sup> and N. Ağırlioğlu<sup>2</sup>

<sup>1</sup> *İskenderun Technical University, Civil Engineering Faculty, Civil Engineering Department, Hydraulics Division, 31200, İskenderun, Hatay -Turkey*

<sup>2</sup> *Istanbul Technical University, Civil Engineering Faculty, Hydraulic Division, 34469, Maslak, İstanbul - Turkey.*

†Corresponding Author Email: [fatih.unes@iste.edu.tr](mailto:fatih.unes@iste.edu.tr)

(Received November 30, 2015; accepted July 4, 2016)

### ABSTRACT

Experimental investigations and observations indicate that water quality modeling is related to the formation of flows in the dam reservoirs. Correct estimation of dam reservoir flow, plunging point and plunging depth are very important for the dam reservoir sedimentation and water quality problem. Therefore, inflow river-water into a dam is modeled in two dimensions through a reservoir with sloping bottom. The model is developed using nonlinear and unsteady continuity, momentum, energy and k- $\epsilon$  turbulence model equations. The equations of the model are solved based on the initial and boundary conditions of the dam reservoir flow for a range of bottom slopes. In addition to velocity, temperature and turbulence viscosity variation through the dam reservoir, the effects of density flow parameters such as plunging depths, plunging points, mixing rate are determined from the simulation results. The results of the present model are compared to the previous experimental works and the mathematical models.

**Keywords:** Density current; Mixing rate; Plunging depth; Densimetric Froude numbers; Reservoir flow; Temporal variation.

### 1. INTRODUCTION

In real reservoir conditions, inflow river water rarely has the same density as the quiescent water in the reservoir. When an inflow of higher density enters ambient dam reservoir water, it plunges below the ambient water and becomes a density underflow. The density difference may be due to the differences in temperature, concentration of dissolved or suspended substances or a combination of both. If river flow enters an ambient dam reservoir waters, then three basic types of currents may occur. These are called the over flow; inter flow, and plunging (density or negatively) flow. If density of incoming flow is smaller than ambient water body in the reservoir, this type of flow will move along the free surface and is called over flow. If reservoir ambient water is stratified due to temperature or other effects, incoming flow will go forward to an intermediate layer whose density is equal to inflow density. This flow is called inter flow. However, if the river water flowing into ambient dam reservoir water is denser than quiescent water density of reservoir, then this type of flow will plunge below the ambient water and will move along the reservoir bottom. This flow is

named as underflow, density negatively flows or plunging flow. The analysis of this flow is very important for reservoir sedimentation studies, water quality modeling and management, effluent mixing analyses and dam reservoir flows characteristic parameters, such as plunging point, mixing rate, circulation flows and etc. in ambient waters.

Real reservoirs do not always have typical geometry due to the variation in volume and shape. If inlet of reservoir has a narrow valley cross-section, then the inflow river water may have little divergence and more slope effects. Conversely, density inflow may affect reservoir divergence. Such features may lead to lateral mixing of the inflow (Üneş, 2010; Farrell and Stefan, 1988).

Plunging phenomenon and density current are very difficult to measure and observe in field and also laboratory conditions. Therefore, only, a few laboratory studies have been performed in the past and those experimental works are not even enough to understand the longitudinal developments of the hydraulic characteristics of density flows throughout the reservoirs. On the other hand, since plunging flow has been studied theoretically using simple models such as two-layer approach in the

past, the momentum equation is used for a part of the flow. These approaches concentrate on the attention only on the plunge region and effectively isolate the plunge region from the rest of the reservoir. Because reservoir flow or density flows process is developed based on hydrodynamic rules throughout the reservoir length, flows are not divided into portions such as plunging region, underflow region and ambient water in real reservoir condition.

Inflow river properties, such as temperature variations and turbidity currents exhibit different models of density currents. In the past, density currents have been observed in field and experimental by many researchers (Wunderlich and Elder, 1973; Chung and Gu, 1998; Mehdizadeh *et al.* 2008, Firoozabadi *et al.* 2010). Experimental studies of density plunging flows over both sloping bottom and diverging horizontal channel were performed by many researchers that most of them established a number of semi empirical equations and used two dimensional reservoir shape (Singh and Shah, 1971, Dallimore *et al.*, 2004). Some of them have been studied the deposition behavior of sediment (Stefan 1973; Lee and Yu 1997; Yu *et al.* 2000).

A few researchers have considered the problem by solving it using numerical methods (Farrell and Stefan, 1986; Fukushima and Watanabe, 1990). They established mathematical models and used numerical solution to investigate the plunging and underflow. In the numerical approach, plunge region needs not to be isolated from the rest of the reservoir so that the river inflow can be simulated along the reservoir. In this solution, plunge region will appear in the emerging flow field as a part of the overall solution. In recent years, researchers used three dimension model simulations and experimental studies to understand the influence of flow inlet condition, density variation and the divergence angle into dam reservoir (Kassem *et al.* 2003, Üneş 2008a, 2008b). Üneş (2010) and Üneş *et al.* (2015) used statistical and mathematical solution and also used artificial intelligence techniques to investigate the plunging flow depth variations. Üneş and Varçin (2012, 2015) developed a hydrodynamics model of an actual dam reservoir in three dimensions for simulating a real dam reservoir flows for different seasons. They defined temperature profiles and flow visualizations and evaluated flow conditions through the real dam reservoir. The solutions gave realistic and useful results for a real dam reservoir.

Several researchers suggested different plunging flow model criteria. In an experimental study performed by Singh and Shah (1971), the reservoir configuration for the process and development of plunge point (Fig. 1) were used. The temporal developments of interfaces between river inflow and ambient water and velocity profiles were only given in the work.

Singh and Shah (1971), Savage and Brimberg (1975), and Akiyama and Stefan (1984) suggested following theoretical equations based on

dimensional analysis, empirical approach, and momentum balance. These relations are used for estimating the plunge depth,  $H_p$ , from mean flow parameters and it is given the following general form (Farrell and Stefan, 1986, 1988).

$$H_p = K \left( \frac{q^2}{g'} \right)^{\frac{1}{3}} \quad (1)$$

where  $K$  is a constant related to the flow conditions;  $q$  is the river discharge per unit width;  $g'$  is reduced gravitational acceleration,  $g' = g \Delta\rho/\rho_0$ , where  $g$  is the acceleration of gravity,  $\Delta\rho = \rho - \rho_0$ ;  $\Delta\rho$  is the density difference between quiescent water and inflow river water,  $\rho$  is inflow river water density and  $\rho_0$  is quiescent water density. From the results of the experimental runs made by Singh and Shah (1971) and the mathematical model of Farrell and Stefan (1988) for estimating the plunge depth,  $H_p$ , the constant  $K$  is found as 1.3 and 1.6, respectively. In the experiments, the densimetric Froude number,  $F_p$ , at the plunge point is defined as:

$$F_p = \left( \frac{q^2}{g' H_p^3} \right)^{\frac{1}{2}} \quad (2)$$

The densimetric Froude number varied over the range from 0.3 to 0.8. Akiyama and Stefan (1984) provided a table summarizing the various formulas for plunge depth prediction. When plunging flow occurs, the inflow river water becomes a density current. This underflow entrains reservoir quiescent water at the interface between inflow and ambient, and proceeds downstream. The dynamics of entraining density current was investigated firstly by Ellison and Turner (1959). They showed that the density current quickly adopts to an equilibrium state due to the constant entrainment rate. Underflow discharge increases along the reservoir due to entrainment. At the run time, reverse current is generated in ambient water because of density flow. The definition sketch of plunging flow and initial entrainment coefficient (Fig. 2) are given by Farrell and Stefan (1988).

Herein,  $H_p$ , is the plunging depth at the plunging point,  $H_d$ , is the depth of the underflow layer,  $U_d$  is underflow layer mean velocity,  $q_d$  is underflow layer stream discharge along the density flow and  $U_{in}$  is river inflow mean velocity (Fig.2).

In this type of flow, the river inflow plunges at a place on ambient reservoir water surface known as plunge point or plunge line. The amount of mixing due to plunging is termed the mixing rate,  $q_{am}/q_{in}$ , and it is always expressed as initial mixing coefficient,  $\gamma$ . The increment of discharge in the density underflow is characterized by this initial mixing rate coefficient at the end of the plunge region,  $\gamma = q_{am}/q_{in}$ , where  $q_{am}$  is the flow rate of entrained ambient water per unit width (the ambient water entrainment rate) or the discharge rate that was entrainment from ambient water to density

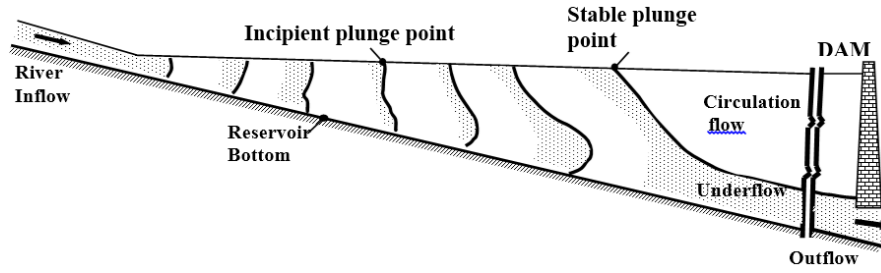


Fig. 1. Development of plunging flow.

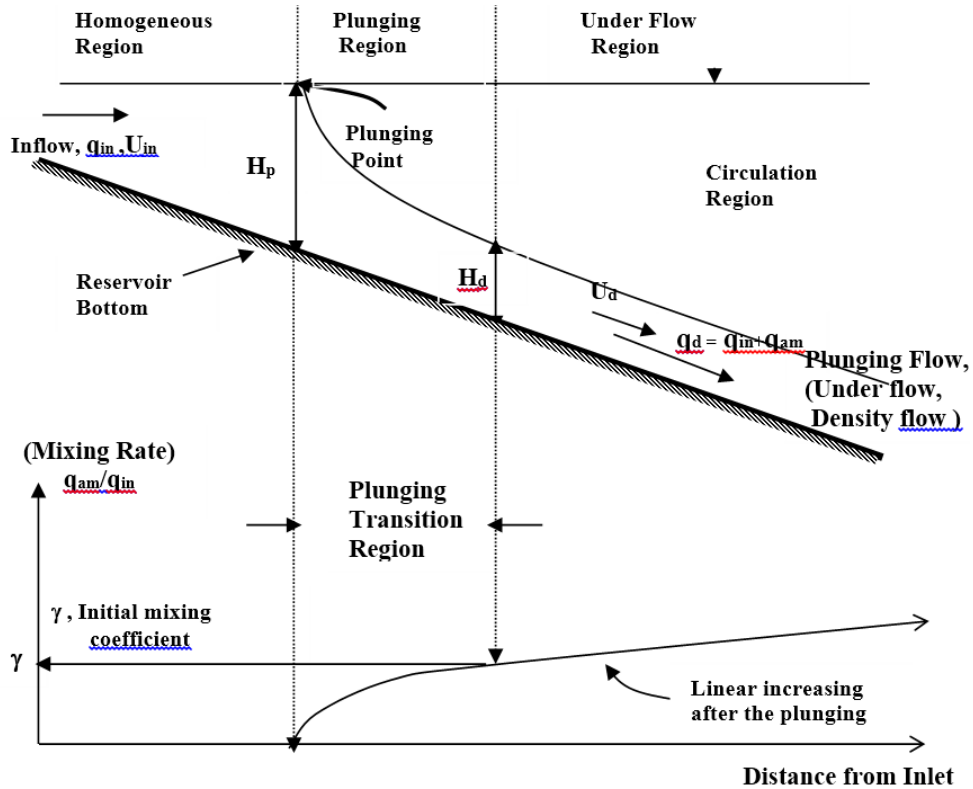


Fig. 2. Sketch of plunging flow and development of mixing rate.

underflow and  $q_{in}$  is the river inflow rate per unit width. The ratio  $q_{am}/q_{in}$  is zero at the plunge point or plunge line and grows abruptly in the plunge region (Fig. 2). Plunge region brings inflow river water from conditions at the plunge line to conditions in the underflow. Therefore,  $\gamma$  is defined as the value of  $q_{am}/q_{in}$  at the end of the plunging region.

In the present study, density plunging (buoyant) flow is investigated and explained with simulation results. The models are applied to condition for a range of flows corresponding to Singh and Shah experimental. The results are compared with the observations made in the experimental runs of Singh and Shah (1971) and the mathematical model of Farrell and Stefan (1986). In this way, variation of velocity, temperature and turbulence viscosity through the dam reservoir, and plunging depths, plunging points, initial mixing rate, mixing

(entrainment) rate along the underflow are determined from the simulation results. Moreover, vertical velocity profiles at the plunging point and along the reservoir, under flow parameters such as densimetric Froude numbers, depths, discharges, velocity, dimensionless discharge and velocity are evaluated. The obtained results can be used reservoir sedimentation studies, water quality modeling and management and effluent mixing analyses.

## 2. MODEL AND FORMULATION

In the current study, solutions and model simulations were obtained for flows corresponding to the experimental runs of Singh and Shah (1971). This experimental reservoir configuration was previously used by Farrell and Stefan (1986) to test their mathematical model. Farrell and Stefan used

cylindrical coordinates and two-dimensional reservoir configuration in their mathematical model.

The reservoir configuration is accommodated in two dimensional (x, y) Cartesian coordinates. Flows such as stratified, plunging and circulation can occur in different density dam reservoir, and these types of flows are very complicated and hard to solve. Therefore, some simplification process has to be made before presenting the governing equations. The assumptions described briefly as in the following parts of the manuscript.

Since this work is limited to two dimensions and so the width of the reservoir is not taken into account, the reservoir shape and divergence effect is not studied. The free surface of the reservoir is modeled as a rigid lid during the proposed model simulation. Therefore, the free surface phenomena such as wind or wave effects are not being considered in reservoir surface. So apart from reservoir geometry, various extraneous forces or factors such as wind, waves and the temperature effects caused by meteorological inputs are not taken into account.

Another simplification is that the temperature difference is taken to be the source of the stratified and buoyancy flows. Field and practice investigation show that the small temperature differences are enough to produce density flow in the reservoir. The density-temperature relation can be linearized and written as follows (Farrell and Stefan, 1986):

$$\Delta\rho = \rho - \rho_0 = \beta\rho_0 [T_0 - T] \quad (3)$$

where  $\rho$  is the water density,  $T$  is the water temperature and  $\beta$  is the coefficient of thermal expansion and calculated as  $\beta = -(\Delta\rho/\rho_0)/(1/\Delta T)$ , where  $\Delta T$  is the temperature difference between ambient and inflow river waters,  $\rho_0$  and  $T_0$  refer to the reservoir conditions. The equation placed into the momentum equation, and Boussinesq approximation and reduced pressure approach is applied as another simplification. At the present time, since reservoir volumes has reached very big and long dimension, the Coriolis force effect is also subject to dam reservoir flow. For this purpose, the Coriolis force effect (Pedlosky, 1987) is included in the mathematical model, though it was so small when compared to the other factors or forces, in the laboratory study. Since the mathematical model is two-dimensional, Coriolis effect is applied only in the x-component of the momentum and energy equations.

Because of the continuous entrainment of ambient water towards downstream, density or plunging flow is analyzed by using unsteady flow mathematical model. The existing model uses eddy (turbulence) viscosities to describe vertical transport due to velocity at the interface on stratified or density flow. To calculate eddy viscosities, k- $\epsilon$  turbulence model approach is used. This method is very useful for the complex reservoirs that have inner circulation and temperature stratified flows. Gorji *et al.* (2014) made a comparative study of turbulence models in a transient channel flow and compared different turbulence models with each

other. Since the density difference occurs due to varying water temperatures, the present mathematical model includes an energy equation for the heat transport. The model equations are solved by using FLUENT software based on the initial and boundary conditions of the reservoir flow.

The mathematical model consists of the following equations: the continuity equation, momentum equations, energy equation and the turbulence model equations (Üneş 2004, 2010; Üneş *et al.* 2015).

*Continuity equation;*

$$\frac{\partial \rho}{\partial t} + \frac{\partial(\rho \bar{u})}{\partial x} + \frac{\partial(\rho \bar{v})}{\partial y} = Sm \quad (4)$$

*Momentum equations;*

For the x axis,

$$\frac{\partial \bar{u}}{\partial t} + \bar{u} \frac{\partial \bar{u}}{\partial x} + \bar{v} \frac{\partial \bar{u}}{\partial y} - f_c \bar{v} = -\frac{1}{\rho_0} \frac{\partial \bar{P}}{\partial x} + \nu_{eff} \left( \frac{\partial^2 \bar{u}}{\partial x^2} + \frac{\partial^2 \bar{u}}{\partial y^2} \right) + \left( \frac{\partial \bar{u}}{\partial x} \frac{\partial \bar{v}}{\partial y} \right) \quad (5)$$

and for the y axis,

$$\frac{\partial \bar{v}}{\partial t} + \bar{u} \frac{\partial \bar{v}}{\partial x} + \bar{v} \frac{\partial \bar{v}}{\partial y} = -\frac{1}{\rho_0} \frac{\partial \bar{P}}{\partial y} + \nu_{eff} \left( \frac{\partial^2 \bar{v}}{\partial x^2} + \frac{\partial^2 \bar{v}}{\partial y^2} \right) + \left( \frac{\partial \bar{u}}{\partial x} \frac{\partial \bar{v}}{\partial y} \right) + g\beta(T_0 - \bar{T}) \quad (6)$$

*Energy equation for the temperature;*

$$\frac{\partial \bar{T}}{\partial t} + \bar{u} \frac{\partial \bar{T}}{\partial x} + \bar{v} \frac{\partial \bar{T}}{\partial y} = \alpha_{eff} \left( \frac{\partial^2 \bar{T}}{\partial x^2} + \frac{\partial^2 \bar{T}}{\partial y^2} \right) \quad (7)$$

where  $\bar{u}$  and  $\bar{v}$  are the mean velocities in the x and y directions, respectively,  $\rho$  is the water density, the source  $Sm$  is the mass added to the continuous phase from the dispersed second phase, such as the effect of water entrainment.  $\bar{P} = \bar{P}' + \rho k (2/3)$ ,  $\bar{P}'$  is the mean pressure adjusted to absorb the hydrostatic portion of the gravity terms,  $k$  is the turbulent kinetic energy and  $\bar{T}$  is the mean temperature,  $f_c$  is the Coriolis parameters,  $\nu_{eff} = \nu + \nu_t$ , where  $\nu$  is the kinematics viscosity and  $\nu_t$  is the kinematics eddy (turbulence) viscosity; and  $\alpha_{eff} = (\nu / Pr) + (\nu_t / \sigma_t)$  is effective thermal diffusivity coefficient; where  $Pr$  and  $\sigma_t$  are the Prandtl and turbulent Prandtl numbers, respectively.

## 2.1 k- $\epsilon$ Turbulence Model Equations

The modified standard k- $\epsilon$  model is used for simulating the effect of turbulence. The model includes the suitable buoyancy terms. Standard k- $\epsilon$  model is based on transport equations for turbulent kinetic energy ( $k$ ) and its dissipation rate ( $\epsilon$ ). k- $\epsilon$  transport model equations have been implemented by Rodi (1980 - 1987). In the derivation of the k- $\epsilon$  model, it was assumed that the flow is fully turbulent, and the effects of molecular viscosity are negligible. Standard k- $\epsilon$  model is therefore valid only for fully turbulent flows. In the present study, FLUENT software is used to solve buoyancy-

extended k-ε turbulence model equations proposed by Rodi (1980). Standard k-ε model in the program is a semi-empirical model of Launder and Spalding (1972) based on model transport equations for turbulent kinetic energy (k) and its dissipation rate (ε).

For a two dimensional unsteady flow at the sloping bottom reservoir, the eddy viscosity  $\nu_t$  is computed from the following equation,

$$\nu_t = C_\mu \frac{k^2}{\varepsilon} \quad (8)$$

where k is the turbulent kinetic energy and ε is the turbulent energy dissipation rate per unit mass. k and ε are obtained from the solution of the following equations in two-dimensional flow (Farrell and Stefan, 1986).

Equation of k

$$\frac{\partial k}{\partial t} + \bar{u}_j \frac{\partial k}{\partial x_j} = \frac{\partial}{\partial x_j} \left[ \left( \nu + \frac{\nu_t}{\sigma_k} \right) \frac{\partial k}{\partial x_j} \right] + \text{Prod} + G - \varepsilon \quad (9)$$

and equation of ε,

$$\rho \frac{\partial \varepsilon}{\partial t} + \bar{u}_j \frac{\partial \varepsilon}{\partial x_j} = \frac{\partial}{\partial x_j} \left[ \left( \nu + \frac{\nu_t}{\sigma_\varepsilon} \right) \frac{\partial \varepsilon}{\partial x_j} \right] + C_{1\varepsilon} \frac{\varepsilon}{k} \text{Prod} - C_{2\varepsilon} \frac{\varepsilon^2}{k} + C_{3\varepsilon} C_3 \frac{\varepsilon}{k} G \quad (10)$$

where Prod is the production of turbulent kinetic energy from the mean flow and is given as

$$\text{Prod} = \nu_t \left( \frac{\partial \bar{u}_i}{\partial x_j} + \frac{\partial \bar{u}_j}{\partial x_i} \right) \frac{\partial \bar{u}_i}{\partial x_j} \quad (11)$$

In these equations, G is the production or destruction of turbulent kinetic energy by buoyancy forces and given as

$$G = g_j \beta \frac{\nu_t}{\sigma_t} \frac{\partial \bar{T}}{\partial x_i} \quad (12)$$

The values of the coefficients  $C_\mu$ ,  $C_{1\varepsilon}$ ,  $C_{2\varepsilon}$ ,  $C_3$ ,  $\sigma_k$ ,  $\sigma_\varepsilon$ , and  $\sigma_t$  appearing in the k-ε turbulence model equations used herein were given the standard values recommended by Launder and Spalding (1974). For the standard k-ε model, these constants are taken as  $C_\mu = 0.09$ ,  $C_{1\varepsilon} = 1.44$ ,  $C_{2\varepsilon} = 1.92$ ,  $\sigma_k = 1.00$ ,  $\sigma_\varepsilon = 1.3$ , and  $\sigma_t = 0.9$ .  $C_3$  is not a part of the standard k-ε model but enters through the buoyancy terms and the constant  $C_3$  is not a stable value.  $C_3$  is not specified, but instead it is calculated according to  $C_3 = \tanh|v/u|$ , where v is the component of the flow velocity parallel to the gravitational vector and u is the component of the flow velocity perpendicular to the gravitational vector (FLUENT User's Guide, 2006).

### 3. BOUNDARY AND INITIAL CONDITIONS

Flow field boundary conditions must be specified individually on the reservoir inlet and outlet planes, at the walls and at the free surface because of unsteady and turbulence reservoir flow. Moreover,

initial fields for each variable must also be specified. Therefore, for each variable, boundary and initial conditions must be chosen individually. This is treated as follows:

- Velocities were given a symmetry condition at the free surface. At the reservoir bottom and dam face, velocities were determined by using the standard wall function that is based on the proposal of Launder and Spalding (1974). This function assumes a log-law velocity profile near the wall and provided in FLUENT as follows.

$$\frac{u_p}{u_*} = \frac{1}{K_\tau} \ln \left( E \frac{u_* y_p}{\nu} \right) - \Delta B \quad (13)$$

where  $u_p$ , mean flow velocity at point p;  $u_*$ , friction velocity;  $K_\tau$ , von Karman constant; E, empirical constant having a value of 9.81;  $y_p$ , distance from point p to the wall; and  $\Delta B$ , roughness function that depends, in general, on the wall roughness height,  $K_s$ . At the inflow boundary, the horizontal velocity component in the x direction, u, is given uniform velocity distribution. The vertical velocity component in the y direction, v, is set to zero. At the outflow point of the reservoir, the horizontal velocity component is allocated a value to exactly balance inflow and the vertical velocity component is taken as zero. The initial velocity field into the reservoir is consisted of a forward horizontal velocity, u, and zero vertical velocity, v, at all points except close to dam.

- The bottom and the free surface of the reservoir's temperatures are taken as adiabatic. The initial temperature field consisted of a constant temperature throughout the reservoir. The dam face temperature is taken equal to the initial temperature of the reservoir water. The inflow river water temperature is set to constant value with no variation over river depth. Reservoir temperature conditions will be changed later during the simulation run time. Therefore, initial temperature values are not of importance.

- In the turbulence model, the k and ε were given a symmetry condition at the free surface same as the velocity condition. Therefore, a zero gradient condition for k was valid at the reservoir bottom and on the dam face. k and ε in the inflow river and near the wall grid points were given a linear profile related to the river shear velocity,  $u_*$ , following the data of Launder and Spalding (1972). At the outflow point, k and ε conditions are the same as the velocity conditions. That is, the zero gradient condition was imposed at the outflow point for k and ε.

### 3.1 Numerical Process

Depending on the appropriate boundary conditions, the problem is solved by using Gambit and computational fluid dynamics solver FLUENT software. The fluxes through the control volume faces are computed by using power law scheme (Patankar, 1980). Before preparing the mathematical model in the program, Gambit is used to draw the experimental reservoir configuration. Mathematical model are solved with the control

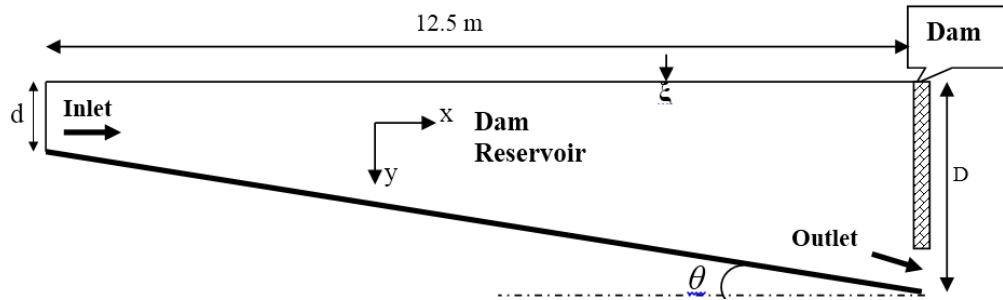


Fig. 3. Schematic projection of model simulation for sloping reservoir.

Table 1 Details of reservoir plunging flow simulations for the present model with Coriolis force

| Run No: | $\theta$ | d (cm) | V (cm/s) | $q_{in}^{in}$ (cm <sup>3</sup> /cm/s) | $T_o$ (°C) | $T_{in}$ (°C) | $(q^2/g')^{1/3}$ (cm) | Farrell & Stefan Model | After Plunge First Appearing |       | After Density Flow Reached the Dam |       |
|---------|----------|--------|----------|---------------------------------------|------------|---------------|-----------------------|------------------------|------------------------------|-------|------------------------------------|-------|
|         |          |        |          |                                       |            |               |                       | $H_p$ (cm)             | $H_p$ (cm)                   | X (m) | $H_p$ (cm)                         | X (m) |
| SSHAH2  | 0.01     | 3.5    | 3.22     | 11.3                                  | 25         | 15            | 4.24                  | 7.7                    | 7.6                          | 3.79  | 8.2                                | 4.06  |
| SSHAH3* | 0.0104   | 8.3    | 3.71     | 30.8                                  | 25         | 15            | 8.27                  | 12.4                   | 12.7                         | 4.3   | 13.83                              | 5.25  |
| SSHAH4  | 0.02     | 16     | 5.95     | 95.3                                  | 18         | 15            | 26.2                  | 35.1                   | 35                           | 9.3   | 37.5                               | 10.23 |
| SSHAH5  | 0.02     | 16     | 3.7      | 59.2                                  | 17         | 15            | 21.8                  | 29.4                   | 29.8                         | 6.71  | 32.3                               | 8.13  |
| SSHAH6  | 0.02     | 8      | 5.3      | 42.1                                  | 18         | 15            | 15.2                  | 22.7                   | 22.1                         | 6.95  | 22.9                               | 7.81  |
| SSHAH7  | 0.02     | 8      | 3.7      | 29.6                                  | 18         | 15            | 12                    | 18.3                   | 18                           | 4.69  | 20                                 | 5.47  |

\* Model run number 3 (Singh and Shah, 1971; and Farrell and Stefan, 1986)

volume approximation by using the software program.

Gambit is used to sketch the reservoir model shape, and than the present mathematical model governing equations is prepared at FLUENT with the appropriate boundary and initial conditions. However, it should be noted that the software programs do not include the Coriolis effect. Therefore, additional user define function is written in C language to include Coriolis effects. When the velocity fields have complex currents such as density flow or circulation flow into the dam reservoir, two types of problems arise. These problems are nonlinear and velocity field–pressure field interdependent. These problems are solved by using the SIMPLE procedure of Patankar and Spalding (1972). This procedure is an iteration method. Since the density flow is unsteady and the run time is too large, the fully implicit scheme is used in the present model to give a stable and realistic solution at large time steps.

#### 4. MODEL DESCRIPTION AND APPLICATION

Density flow has been studied with a sloping reservoir bottom. Basic model data are taken from

the experimental data of Singh and Shah (1971) and model of Farrell and Stefan (1986). Experimental reservoir configurations of both studies are taken from papers and project report (Fig. 3). In addition, different inflow densimetric Froude numbers and slopes are taken and investigated herein. Density differences are generated using water of different temperatures for quiescent and inflow river water.

In this model figure, dam reservoir length is 12,5 m;  $\theta$  is dam reservoir channel bottom slopes (0.01-0.02); d is the reservoir inflow channel depths (3.5 - 16 cm); and D is dimensions of the model outlet (16 - 41cm). All the parameters used in the model (depth and changing reservoir bottom slopes, and other flow parameters) are given in Table 1. The independent variables governing the density flow in sloping dam reservoir channel and six cases model runs considered in this study are also shown in Table 1. These cases correspond to experimental data of Singh and Shah (1971) and model of Farrell and Stefan (1986). In Table.1, V, is the mean inflow velocity;  $q_{in}$ , is inflow discharge;  $H_p$ , is plunging depth; X, is the distance from reservoir inlet;  $T_o$  and  $T_{in}$  are inflow and ambient water temperature respectively.

The computational domains are divided into 125



and 17 grids in the x and y directions, respectively. As an initial model condition, the inflow channel is first filled with warm water, and then the cold water is released at the upstream end of the inflow channel at a specified rate. The current proceeds forward until it reaches to the downstream boundary. The inlet densimetric Froude number in all cases exceeds unity, indicating an incoming supercritical flow condition. The calculation is continued for approximately 800 s at which point the front has long past the downstream boundary and any change in the flow field would be insignificant. In order to have the desired converged solution, a time step of 10 seconds was chosen after the preliminary trials

## 5. RESULTS

In this study, mathematical model simulations were carried out at a range of flow conditions. These simulations yielded realistic plunging flow fields in all runs and were developed in a similar manner as described by Singh and Shah (1971) and Farrell and Stefan (1986) model results. The details of these runs are given (Table 1). The results obtained for each variable are evaluated as follows.

### 5.1 Dam Reservoir Parameters

#### 5.1.1 Plunge Depth

The plunge points are taken as the position where plunging first appears. Plunging flow, details of numeric simulations and extracted plunge point depths are given for different bottom slopes and condition (Table 1). Since Singh and Shah gave only details of one experiment for run SSHAH3, the run SSHAH3 are used for the present model and compared with the model results. The experimental plunging depth of SSHAH3 is the same magnitude as that from the present model and is equal to 12.7 cm; however, for this run, Farrell and Stefan model give an error of 2.4%. The plunge depths from the present study,  $H_p$ , are plotted against  $(q^2/g')^{1/3}$  which is the parameter used by Singh and Shah (1971) to correlate their experimental data (Fig. 4). These results are fitted to a line and also given K coefficient in Equation (1) is extracted from the figure for the present model simulations.

The K multiplier is found to be 1.3 by Singh and Shah (1971) experimental predictions and 1.6 by Farrell and Stefan (1988) numerical simulation results. K multiplier is found as 1.39 in the present mathematical model simulations. The mathematical model result is very close to the experimental measurement. In order to compare the present plunge depths variation and compatibility with other study, the obtained model results are plotted along with Singh and Shah (1971) and Farrell and Stefan (1986) results (Fig. 5). As it can be seen clearly from the graphs, a good correlation was obtained between  $H_p$  and  $(q^2/g')^{1/3}$  for the present two dimensional model.

Plunge depth and plunge point distance from inlet are given as  $H_p$  and X (Table 1), respectively. The plunging depth and the plunging distance from inlet

are found to increase within the ranges of 3.5 – 10 % and 6 – 18 % between plunging first appearing and density flowing reached the dam, respectively. The reasons of such increment are the density flow development in the reservoir, reservoir bed slope and the plunging flow dynamics.

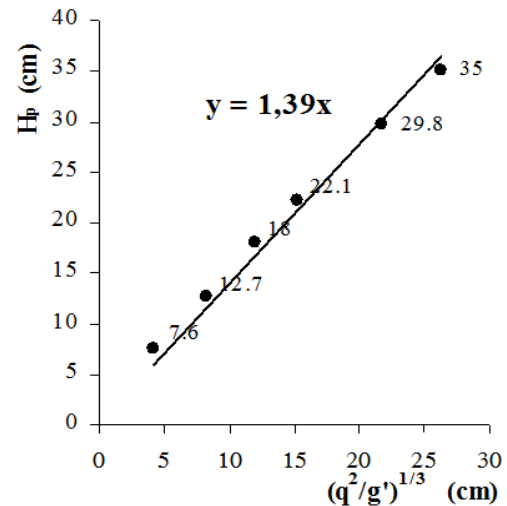


Fig. 4. Plunge depths from the present numerical simulation.

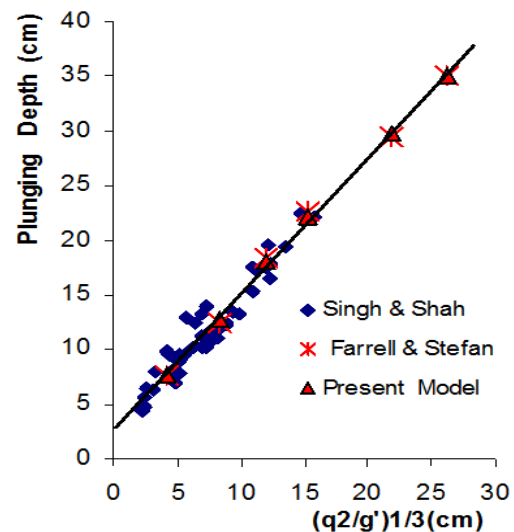
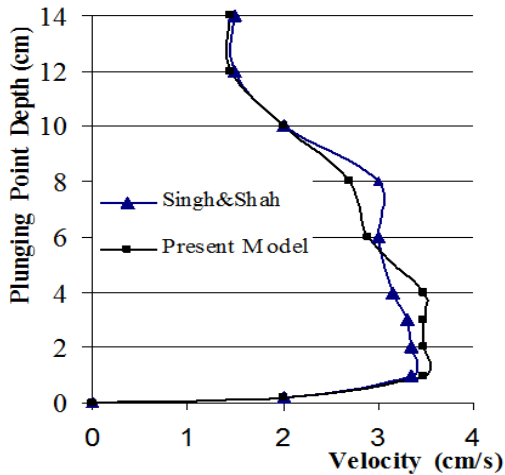


Fig. 5. Comparison of the present numerical model simulations with the previous studies.

#### 5.1.2 Variation of Vertical Velocity Profiles at the Plunging Point

A few researchers investigated the plunging phenomenon experimentally and theoretically, but only Singh and Shah (1971) gave velocity profile distribution in plunging point based on one experimental condition. Therefore, those data are used for comparison of experimental and numerical model velocity profiles near the plunge point (Farrell and Stefan, 1986). The model was developed using the flow and geometric conditions given for run SSHAH3. As a result of this model, a plunging depth

of 12.7 cm was found. This depth corresponds well with the value determined in the experiments. The maximum percentage difference between the present model results and experimental velocity values is about 11%, which is in the acceptable limit (Fig.6). The comparison of these profiles shows an excellent agreement between the experimental values and the present model simulations.



**Fig. 6. Comparison of experimental and numerical velocity profiles near the plunge point, for run SSHAH3.**

### 5.1.3 Variation of Vertical Velocity Profiles Along the Reservoir

Development and advance of density flow and vertical velocity profiles for different sections can be seen graphically (Figs. 7 a, b and c) at different distances from inlet. Velocity profiles are investigated at three different sections ( $X/L = 0.5, 0.75$  and  $1.0$ ). In the graphics,  $X$  is the distance from inlet and  $L$  is the reservoir length.

These figures show comparisons among the model with Coriolis Effect and without Coriolis force effect for run SSHAH3 model data, and at the 600 seconds elapsed time. In model with Coriolis force, velocities to downstream direction are less than those of model without Coriolis force. Similarly, velocities in upstream direction in Coriolis model are less than those of the model without Coriolis. As seen from vertical velocity profiles (Figs. 7 a, b and c), although inlet velocities are 3.71 cm/s, mean velocity distribution of Coriolis model for the selected cross sections varies between  $-0.66$  and  $5.5$  cm/s. On the other hand, without Coriolis model it varies between  $-0.3$  and  $5.5$  cm/s. The negative velocities are shown in the circulation zone and the velocities vary between  $0.3$  and  $1.45$  cm/s. Stratified and under flow development can be clearly seen at the present profiles.

### 5.1.4 Temporal Variation of Velocity Field

The velocity fields obtained from models are developed in a similar manner as both the available experimental and mathematical model results. In all run simulations, initially the inflow

river cold water advanced into the reservoir, pushed forward under the ambient warm water and then the warm water is displaced forward and the velocities are in the downstream direction at all points. The warm water is initially displaced forward and velocities are forward at all points. When the denser cold water pushed slightly forward under the warm water, consequently a small region of (back) recirculation flow appeared in the ambient water surface. In this way plunging flow started and then the river inflow cold-water flow downstream under the ambient warm water as a density current. This backflow region grew larger as time elapsed and then eventually the density current front reached the dam base and the entire ambient warm water zone is transformed into a recirculation zone and a stratified flow is produced along the reservoir.

Typical velocity fields for the runs of SSHAH3 at different elapsed times are given from the simulation results. The simulation results are given the vectors and contours of the velocity fields. Plunge point is well defined in these simulation velocity fields. Times in the development of flows are presented (Figs. 8 to 10). These fields illustrate the different elapsed times that are used in the initial stage and the density flow that reaches to the dam.

The initial condition velocity field and the flows are in the downstream direction at all points (Figs. 8 a- b). Velocity vector and contour field are defined in the simulations for the elapsed time 210 seconds after plunging (Figs. 9 a- b). The situation at that time is just the appearance of a small region of backflow over the plunging flow where the underflow velocities are about 4.68 cm/s (Fig. 9).

The density flow reached to the dam face at the elapsed time of 600 seconds and at the same time, recirculation region reached to the dam too (Figs. 10 a- b ). The recirculation region grows and covers the entire reservoir and maximum velocities appear in the under flow region. Plunge point and region of recirculation flow is well defined and shown in these simulation velocity fields. The velocities in the model simulations increase from 3.71 cm/s to 5.60 - 5.79 cm/s during the run elapsed time. The reason for the velocity increment can be explained with the increase of bottom slope and with charging balance of force. This feature is appeared in all the other model simulations and experimental measurements. Thus, all results show development of circulation zone and plunging depth typical velocity contour and vector fields for the runs of SSHAH3. As seen from the model simulation and velocity field development, dilution and reduction in density in downstream direction is observed during this process.

### 5.1.5 Temporal Variation of Temperature Field

Contours of the temperature field development are defined with simulations for run SSHAH3 at the particular elapsed times (Figs. 11 a- b). The



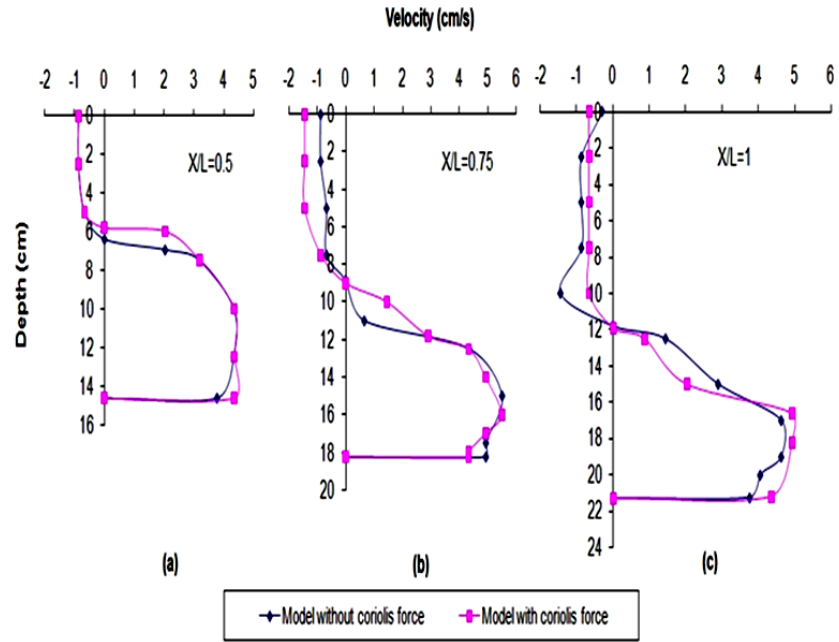


Fig. 7. Vertical velocity profiles at the downstream of the plunge point (a) for  $X/L=0.5$ ; (b) for  $X/L=0.75$ ; and (c) for  $X/L=1.0$  (Run SSHAH3, elapsed time is 600 seconds).

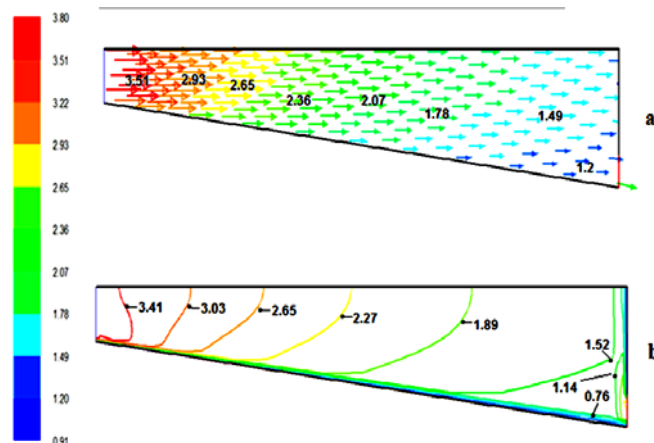


Fig. 8. Typical initially flow velocity: a) Vector field; b) Contour field, (elapsed time is 30 seconds).

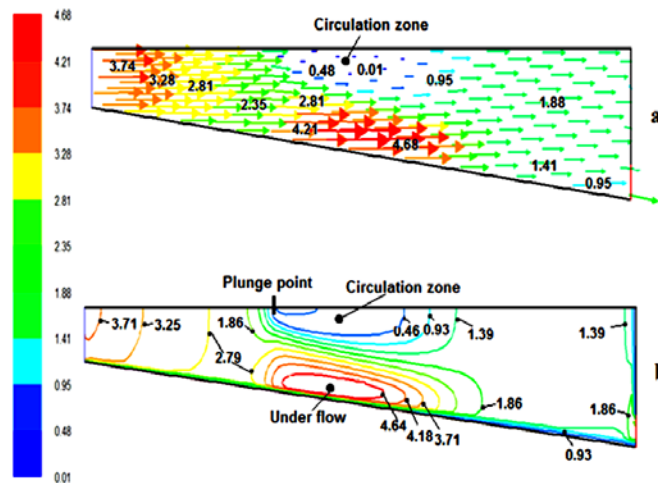


Fig. 9. Reservoir velocity: a) Vector field; b) Contour field at initiation of circulation flow for experimental SSHAH3 (elapsed time is 210 seconds).

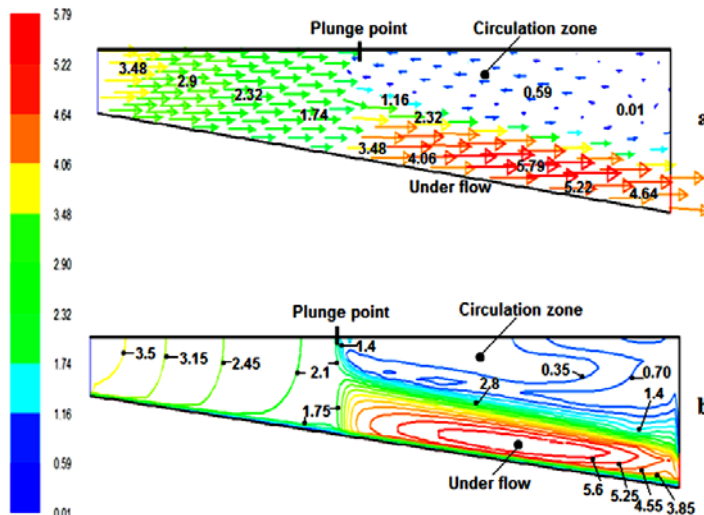


Fig. 10. Reservoir velocity: a) Vector field; b) Contour field after density flow reached the dam for experimental SSHAH3 (elapsed time is 600 seconds).

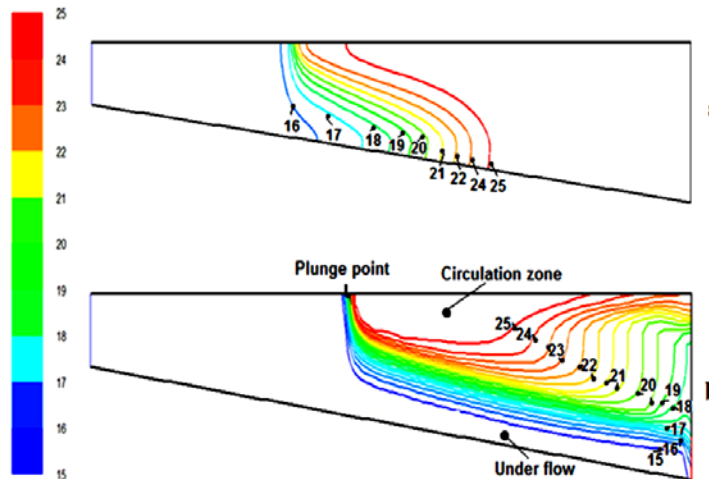


Fig. 11. Reservoir temperature contours (°C) field: a) Initiation of circulation flow for experimental SSHAH3 (elapsed time is 210 seconds); b) After the density flow reached dam for experimental SSHAH3 (elapsed time is 600 seconds).

temperature contour lines on those figures are suitable for either the velocity vector and contour fields or the limits of the recirculation region. Reservoir model temperature varied between inflow (15°C), and ambient water temperature (25°C) range. The temperature variation occurs after the plunging point and in stratified flow region.

The behavior of plunging flow can be seen on those temperature counter lines such as velocity fields. Both temperature and velocity contours show clearly the upwelling of mixed water at the reservoir. The plunge point in the velocity and temperature fields appears stable but it is drifted continuously a small amount towards the downstream. It is associated likely with the charging balance of forces as the density current moves downstream the reservoir bottom. Therefore, the plunge point and depth never stabilized and plunge point continued to move towards the dam.

### 5.1.6 Variation of Turbulence (eddy) Viscosity

As with the other models, the reservoir flow is developed in a similar manner in all the turbulence simulation runs. In initial stages of a typical run, flows are forwarded at all points and turbulence (eddy) viscosity in the order of  $10^{-3}$  -  $10^{-4}$   $m^2/sec$  developed through the reservoir. The resulting density gradients give rise to a local lowering of  $\nu_t$  values in the reservoir. Stratified flows, plunging point, and recirculation zone developed in that area of low turbulence viscosity. Longitudinal cross-section profiles of turbulence viscosity ( $\nu_t$ ) are found with simulation results (Figs.12 a- b).

Turbulence viscosity fields at the development of initial circulation flow for run SSHAH3 are determined (Fig.12 a). Turbulence viscosity fields for run SSHAH3 just as the cold waterfront reaches

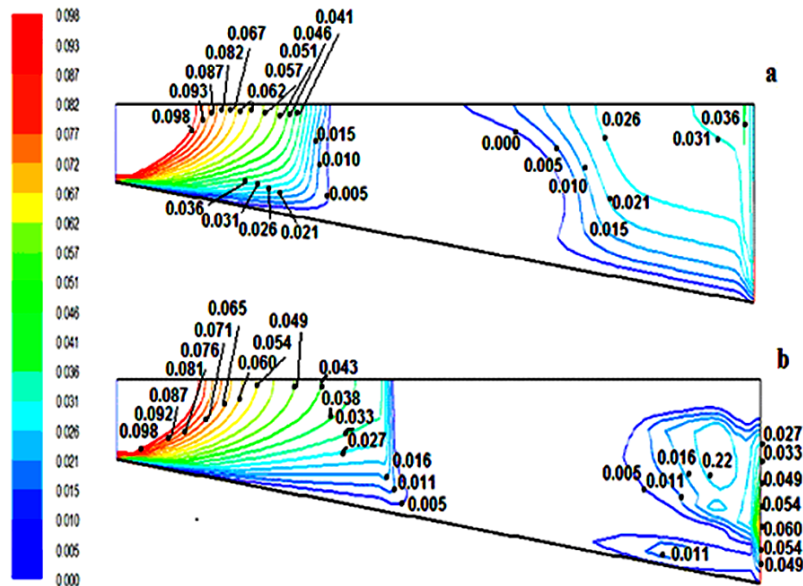


Fig. 12. Reservoir turbulence viscosity fields: a) Initiation of circulation flow for experimental SSHAH3 (elapsed time is 210 seconds); b) After the density flow reached dam for experimental SSHAH3 (elapsed time is 600 seconds).

Table 2 Underflow parameters for reservoir numerical simulation run (Run SSHAH3, Elapsed time 600 seconds)

| X   | $q_{in}$        | $q_d = q_{am} + q_{in}$ | $U_d$      | $H_d$ | $F_d$ | $q_{am} / q_{in}$ |
|-----|-----------------|-------------------------|------------|-------|-------|-------------------|
| (m) | ( $cm^3/cm/s$ ) | ( $cm^3/cm/s$ )         | ( $cm/s$ ) | (cm)  |       |                   |
| 2   | 30.8            | 30.8                    | -          | -     | -     | -                 |
| 4.3 | 30.8            | 30.8                    | -          | -     | -     | -                 |
| 6   | 30.8            | 34.43                   | 3.89       | 8.85  | 1.01  | 0.11              |
| 8   | 30.8            | 41.91                   | 4.58       | 9.15  | 1.17  | 0.36              |
| 10  | 30.8            | 44.10                   | 4.69       | 9.4   | 1.18  | 0.43              |
| 12  | 30.8            | 44.36                   | 4.69       | 9.46  | 1.18  | 0.44              |

to the dam are displayed (Fig.12 b). The results indicate that the  $G$  term in  $k$  equation (Eq. 9) grows larger and  $\nu_t$  disappears effectively over much of the recirculation flow zone (Farrell and Stefan, 1986). Therefore, the lowering of eddy viscosity appears to be an essential part of the plunging flow physics (Fig. 12 a-b).

### 5.1.7 Variation of Density Current Parameters

Underflow discharge, velocity distribution, and depths variations are determined from the model simulation results. The entrainment water quantity that is carried from ambient water to density underflow can be determined from model simulations. Underflow discharge and other underflow parameters for run SSHAH3 at the 600 seconds elapsed time are computed along the reservoir and given in the table (Table 2). In the table;  $q_{am}/q_{in}$  is mixing rate;  $q_{in}$  is the river inflow rate per unit width;  $q_{am}$  is the increase in discharge

rate per unit width of the underflow;  $q_d = q_{in} + q_{am}$ ,  $q_d$  is underflow layer stream discharge;  $H_d$  is underflow layer depth;  $U_d$  is underflow layer mean velocity;  $F_d$  is underflow layer densimetric Froude number, and  $\gamma$  is Initial mixing coefficient.  $\gamma$  and  $(q_{am}/q_{in})$  were extracted from simulation result of SSHAH3.

The  $q_{am}/q_{in}$  values are plotted against the distance along the reservoir (Fig. 13). Since the initial mixing coefficient is the value of  $q_{am}/q_{in}$  where the underflow starts,  $\gamma$  value is found as 0.11 (Table 2). As expected, the  $q_{am}/q_{in}$  values are found to increase along the reservoir.

Variations of dimensionless velocity and discharge along the reservoir are found model simulation (Fig.14). Mean underflow velocity increases along the density underflow. Since underflow current starts after plunging, mean velocity and discharge are taken zero until the plunging point is reached (Fig.14). The model results are found to be the same

development and magnitude as the experimental measurement.

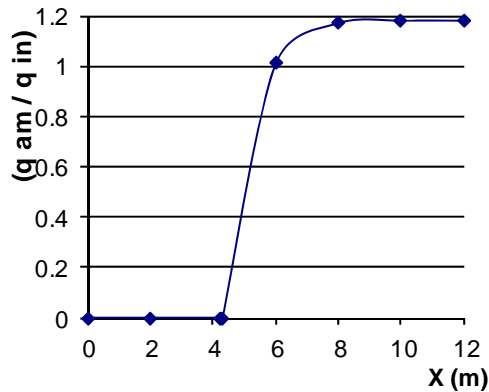


Fig. 13. Typical longitudinal variations of mixing rate (Run SSHAH3).

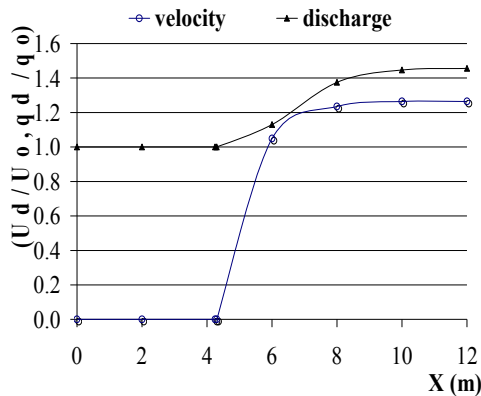


Fig. 14. Typical longitudinal variations of dimensionless velocity and discharge.

Variation of the underflow depth along the model reservoir are determined with the model simulation (Fig.15 a). It can be seen the results that the under flow depth ( $H_d$ ) increase linearly according to the bottom slope of the stratified flow. Typical longitudinal variations of underflow densimetric Froude numbers,  $F_d$ , is given (Fig.15 b). The inlet densimetric Froude number in all cases exceeds unity. The  $F_d$  variation indicate that underflow along the model reservoir are formed supercritical flow condition.

## 6. CONCLUSIONS

A mathematical model including Coriolis force is derived to investigate the characteristic parameters of density flow in a dam reservoir. The mathematical model is solved numerically and simulated. In the present numerical approach, plunge region need not be isolated from the rest of the reservoir so that the river inflow can be simulated along the reservoir. In this solution, plunge region and so other flow parameters will appear in the emerging flow field as a part of the overall solution.

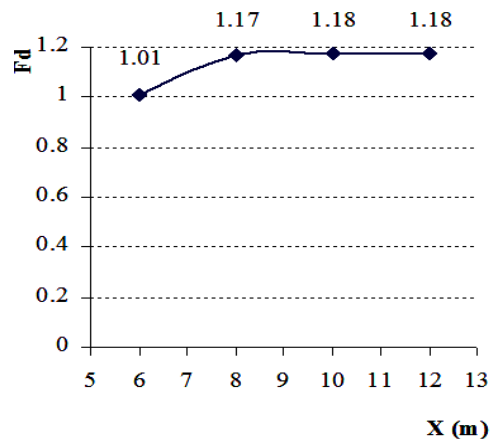
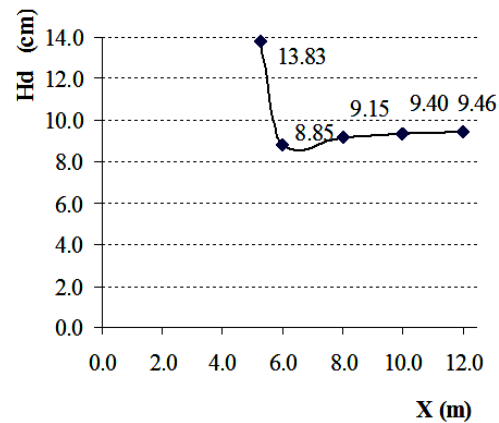


Fig. 15. Typical longitudinal variations of (a) Underflow depth ( $H_d$ ); (b) Underflow densimetric Froude numbers.

The model results are compared with the experimental data obtained from Singh and Shah (1971). The agreement between the model results and the experimental data is found to be promising. Specifically, the following observations and conclusions can be made:

The simulation results obtained from this study compared with previous experimental work and the mathematical model studies data on density current generated by the plunging of cold water in ambient warm water. The results show that model forecasts are much closer to the experimental measurements.

Developed mathematical model appear to be able to successfully simulate turbulent density flow in different slope channels. The model simulation results were analyzed to determine density flow characterizing parameters such as plunging points, plunging depths, plunging distance from reservoir inlet, initial mixing rate, turbulence effects, mixing (entrainment) rate along the underflow. Furthermore, variations of underflow depths, velocity, temperatures and turbulence viscosity through the dam reservoir can be determined.

As seen in the mathematical model, the effective gravitational force is the main driving force in density current. The velocity and flow profiles are closely related to the density profile in the reservoir.

The mathematical model including Coriolis effect

appear to be able to successfully simulate turbulent density flow in a reservoir channel. Therefore, effects of Coriolis force on velocity fields and plunging point are also investigated and evaluated graphically.

Density and stratified flow are greatly affected by reservoir bed slope, densimetric Froude number of the inflow, temperature variation and consequently reservoir shape. However, simulation results illustrate that channel bottom slope is obviously an important parameter for defining development of plunging depth and region. Another important point is that when bottom slope is less than  $1^\circ$ , the occurrence of stratified flow becomes difficult.

The plunging depth and the plunging distance from the inlet are found to be increasing within the ranges of 3.5 – 10% and 6 – 18% between the plunging first appeared and the density flow just reaching the dam, respectively. The reasons of increment are due to reservoir bed slope and the plunging flow dynamics. The other comparison parameter, plunging depth constant,  $K$ , is found to be very close to each other which are 1.30 for the experimental measurement and 1.39 in the present mathematical model. Experimental and model velocity profile distributions in plunging point are defined and the maximum percentage is found around 11%. These parameters showed an excellent agreement with the ones found in the previous studies. Furthermore, plunging flow, density flow and recirculation zone development can be well defined in the velocity, temperature and turbulence fields in the model simulation figures. Therefore, the present model simulations provide useful insight for understanding and determining plunging flow patterns as well as density flow in any point along the dam reservoir.

Those findings are very promising that the mathematical model simulations as well as results obtained can be used in the studies related to dam reservoir such as sedimentation, water quality modeling, mixing analyses, water contamination and management.

## REFERENCES

- Akiyama, J. and G. H. Stefan (1984). Plunging flow into a reservoir theory. *Journal of Hydraulic Engineering* 110, 484-489.
- Chung, S. W. and R. Gu (1998). Two dimensional simulations of contaminant currents in stratified reservoir. *Journal of Hydraulic Engineering* 124, 704-711.
- Dallimore, C. J., J. Imberger and B. R. Hodges (2004). Modeling a plunging underflow. *Journal of Hydraulic Engineering* 130(11) 1068-1076.
- Ellison T. H. and J. S. Turner (1959). Turbulent entrainment in stratified flows. *Journal of Fluid Mechanics* 6, 423.
- Farrell, G. J. and H. G. Stefan (1986). Buoyancy Induced Plunging Flow into Reservoirs and Coastal Regions. *Minnesota Project Report* 241.
- Farrell, G. J. and H. G. Stefan (1988). Mathematical modeling of plunging reservoir flows. *Journal of Hydraulics Research* 26, 525-537.
- Firoozabadi, B., H. Afshin and A. Bagherpour (2010). Experimental investigation of turbulence specifications of turbidity currents. *Journal of Applied Fluid Mechanics* 3, 63-73.
- FLUENT 6.3 User's Guide, 2006, FLUENT incorporated
- Fukushima, Y. and M. Watanabe (1990). Numerical simulation of density underflow by the  $k-\epsilon$  turbulence model. *J. Hydroscl. Hydr. Eng.* 8, 31-40.
- Gorji, S., M. Seddighi, C. Ariyaratne, A. E. Vardy, T. O'Donoghue, D. Pokrajac and S. He (2014). A comparative study of turbulence models in a transient channel flow. *Computers and Fluids* 89, 111-123.
- Kassem, A., J. Imran and J. Khan (2003). Three-dimensional modeling of negatively buoyant flow in diverging channels. *Journal Hydraulic Engineering* 129(12), 936-947.
- Lauder, B. E. and D. B. Spalding (1972). *Mathematical Models of Turbulence*, Academic Press, New York.
- Lauder, B. E. and D. B. Spalding (1974). The Numerical Computation of Turbulent Flows. *Computer Methods in Applied Mechanics and Engineering* 3, 269-289
- Lee, H. Y. and W. S. Yu (1997). Experimental study of reservoir turbidity current. *Journal Hydraulic Engineering* 123(6), 520-528.
- Mehdizadeh, A., B. Firoozabadi and B. Farhanieh (2008). Numerical simulation of turbidity current using  $v^2 - f$  turbulence model. *Journal of Applied Fluid Mechanics* 2, 45-55.
- Patankar, S. V. (1980). *Numerical Heat Transfer and Fluid Flows*, McGraw-Hill, New York.
- Patankar, S. V. and D. B. Spalding (1972). A calculation procedure for heat mass and momentum transfer in three dimensional parabolic flows international. *Int. Journal Heat and Mass Transfer* 15(10), 1517-1806.
- Pedlosky, J. (1987). *Geophysical Fluid Dynamics*, Springer-Verlag, New York.
- Rodi W (1980) Turbulence Models and Their Application in Hydraulics, Report International Assoc. for Hydraulic Research, Delft, Netherlands.
- Rodi, W. (1987). Example of calculation methods for flow and mixing in stratified fluids. *J. Geophys. Res.* 92, 5305-5328.

- Savage, S. B. and J. Brimberg (1975). Analysis of plunging phenomena in water reservoirs. *J Hydr. Res.* 13(2), 187-204.
- Singh, B. and C. R. Shah (1971). Plunging Phenomenon of Density Currents in Reservoirs. *La-Houille Blanche* 26, 59-64.
- Stefan, H. G. (1973). High concentration turbidity currents in reservoirs. *IAHR* 1, 341-352.
- Üneş, F. (2004). *Investigation of Effects of Coriolis Forces and Outlet Levels on Reservoir Flow Using Mathematical Model*, Istanbul Technical University. Ph. D. Dissertation, Institute of Science and Technology, Istanbul, Turkey.
- Üneş, F. (2008a). Investigation of density flow in dam reservoirs using a three-dimensional mathematical model including Coriolis effect. *Computers and Fluids* 37, 1170-1192.
- Üneş, F. (2008b). Analysis of plunging phenomenon in dam reservoirs using three dimensional density flow simulations. *Canadian Journal of Civil Engineering* 35, 1138-1151.
- Üneş, F. (2010). Prediction of density flow plunging depth in dam reservoir an artificial neural network approach. *Clean –Soil Air Water* 38(3), 296-308.
- Üneş, F., D. Joksimovic and O. Kisi (2015). Plunging flow depth estimation in a stratified dam reservoir using neuro-fuzzy technique. *Water Resour Manage* 29, 3055–3077
- Üneş, F. and H. Varçin (2012). Investigation of plunging depth and density currents in Eğrekkaya dam reservoir, Turkish Chamber of Civil Engineers. *Technical Journal (Teknik Dergi)* 1, 5725- 5750.
- Üneş, F. and H. Varçin (2015). Investigation of seasonal thermal flow in a real dam reservoir using 3-d numerical modeling. *Journal of Hydrology and Hydromechanics* 63(1), 38-46.
- Wunderlich, W. O. and R. A. Elder (1973). *Mechanics of flow through man-made lakes*. American Geophysical Union, Washington DC.
- Yu, W. S., H. Y. Lee and S. H. M. Hsu (2000). Experiments on deposition behavior of fine sediment in a reservoir. *Journal Hydraulic Engineering* 126(12), 912-92.